



Electroacupuncture ameliorates cognitive impairment in APP/PS1 mouse by modulating TFEB levels to relieve ALP dysfunction

Haotian Chen^a, Xiaokun Yang^a, Yushan Gao^b, Huili Jiang^a, Mengwei Guo^a, Yingyi Zhou^a, Chenlu Li^a, Yunxiang Tan^c, Yang Zhang^d, Weiguo Xue^{a,*}

^a School of Acupuncture-Moxibustion and Tuina, Beijing University of Chinese Medicine, Beijing 100029, China

^b School of Traditional Chinese Medicine, Beijing University of Chinese Medicine, Beijing 100029, China

^c The First Affiliated Hospital of Guangzhou University of Chinese Medicine, 510405, China

^d Guangshui City Hospital of Traditional Chinese Medicine, 432700, China



ARTICLE INFO

Keywords:

Alzheimer's disease
Electroacupuncture
APP/PS1 mice
Autophagy-lysosomal pathway
Transcription factor EB

ABSTRACT

Recently, the underlying mechanisms of acupuncture on the effects of Alzheimer's disease (AD) treatment have not been fully elucidated. Defects in ALP (autophagy-lysosomal pathway) and TFEB (transcription factor EB) play critical roles in AD. Our previous studies have demonstrated that electroacupuncture (EA) can ameliorate both β -amyloid ($A\beta$) pathology and cognitive function in APP/PS1 mice.

However, the effects of EA on the expression of ALP and TFEB and their potential mechanisms require further investigation.

Twenty-eight male APP/PS1 mice were randomly divided into Tg and Tg + EA groups, and 14 C57BL/6 mice served as the wild-type (WT) group. After 1 week of adaptation to the living environment, mice in the Tg + EA group were restrained in mouse bags and received manual acupuncture at Baihui (GV20) acupoint and EA stimulation at bilateral Yongquan (KI1) acupoints, using the same restraint method for WT and Tg groups. The intervention was applied for 15 min each time, every other day, lasting for six weeks.

After intervention, the spatial learning and memory of the mice was assessed using the Morris water maze test.

Hippocampal $A\beta$ expression was detected by immunohistochemistry and ELISA. Transmission electron microscopy (TEM) was used to observe autophagic vacuoles and autolysosomes in the hippocampus. Immunofluorescence method was applied to examine the expression of TFEB in CA1 region of the hippocampus and the colocalization of CTSD or LAMP1 with $A\beta$. Western blot analysis was performed to evaluate the changes of LC3, p62, CTSD, LAMP1, TFEB and n-TFEB (nuclear TFEB) in the hippocampus.

The findings of behavioral assessment indicated that EA alleviated the cognitive impairment of APP/PS1 mice. Compared with the WT group, the Tg group showed significant cognitive decline and abnormalities in ALP and TFEB function ($P < 0.01$ or $P < 0.05$). However, these abnormal changes were alleviated in the Tg + EA group ($P < 0.01$ or $P < 0.05$). The Tg group also showed more senile plaques and ALP dysfunction features, compared with the WT group, and these changes were alleviated by EA.

In conclusion, this study highlights that EA ameliorated $A\beta$ pathology-related cognitive impairments in the APP/PS1 model associated with ALP and TFEB dysfunction.

1. Introduction

Alzheimer's disease (AD) is a degenerative disease of the central nervous system, which is the most common form of dementia, accounting for approximately 60 % of all dementia cases (2022; Gauthier et al., 2022). Studies have shown that the senile plaques (SPs) and neurofibrillary tangles (NFTs) caused by amyloid- β and tau proteins are

the main pathological features of AD (Lane et al., 2018). Clinically, AD is characterized by memory impairment, aphasia, or apraxia, etc., which might result in reduced ability to perform daily activities and mental abnormalities (2022; Gauthier et al., 2022).

According to a report from WHO (World Health Organization), the number of AD patients in 2019 was about 55 million and is predicted to increase to 139 million by 2050 (2022). As the world's population ages,

* Corresponding author.

E-mail address: snowmanxue@126.com (W. Xue).

the number of people with AD will increase rapidly, posing a significant challenge to society and healthcare systems. There is an urgent need for effective methods to delay or reverse the progression of AD.

The pathogenesis of AD is complex, and the A β cascade hypothesis is considered to be the major pathogenic hypothesis of AD (Karran et al., 2011). Data from the experimental investigation has implied that the neurotoxic substance A β is mainly produced by neurons in the brain and accumulates within neurons, which can lead to impairment of axonal function and synaptic plasticity (Eimer and Vassar, 2013; Yang et al., 2022).

While the A β cascade hypothesis alone is considered to be not yet sufficient to explain the pathogenesis of AD, recent studies have found that the dysfunction of the autophagy-lysosomal pathway is one of the earliest pathological changes in AD and believed to play a key role in the A β pathology (Liang and Jia, 2014; Nixon and Yang, 2011). Increasing genetic and epidemiologic evidence has suggested that severe ALP (autophagy-lysosomal pathway) impairment is an important trigger in the development of AD and may accelerate the production of A β (Yang et al., 2022; Lee and Nixon, 2022; Nixon, 2007; Rahman et al., 2021). ALP has been investigated to be highly active in neurons and has the ability to clear misfolded and aggregation-prone proteins such as A β , suggesting that regulation of ALP may be beneficial in AD (Caccamo et al., 2010).

ALP is particularly important in neurons, which cannot clear toxic fragments and damaged organelles through cell division (Uddin et al., 2019). The sophisticated mechanism of ALP regulation involves multiple signaling pathways and factors, including the TFEB (transcription factor EB), which can regulate ALP's functional activity at the level of gene expression (Sardiello et al., 2009).

TFEB is considered to be one of the principal transcriptional regulators of autophagy and is widely expressed in the central nervous system. It is usually localized in the cytoplasm in an inactive phosphorylated state. However, upon starvation or impaired lysosomal function, TFEB can be dephosphorylated and translocated to the nucleus to selectively bind to the CLEAR (Coordinated Lysosomal Expression and Regulation, CLEAR) motif, which is abundant in the promoters of autophagy and lysosome-related genes (Sardiello et al., 2009; Cortes and La Spada, 2019; Settembre et al., 2011).

TFEB and its associated activities have been reported to be altered in AD, which decreased the levels of TFEB in the nucleus but not in the cytoplasm (Reddy et al., 2016; Wang et al., 2016). Simultaneously, the expression of both TFEB and its target ALP genes and proteins is reduced due to suppressed CLEAR network activity (Tiribuzi et al., 2014). An increasing number of studies have indicated that the upregulation of TFEB levels in the brain has a positive effect on ALP, thereby attenuating A β pathology in AD (Bao et al., 2016; Xiao et al., 2014; Xiao et al., 2015).

Therefore, the selection of appropriate instruments to strengthen the function of TFEB and consequently improve the ALP defects in AD might be a new way for the prevention and treatment of AD.

Acupuncture and electroacupuncture are widely used as a highly acknowledged complementary treatment for various neurodegenerative diseases (Wu et al., 2023; Ye et al., 2017). Relevant clinical and animal research has shown that acupuncture has a positive effect on AD, and acupuncture can alleviate the general clinical symptoms and cognitive function of AD patients with a relatively safe and well-tolerated method (Cao et al., 2016; Du et al., 2022; Jia et al., 2017; Zheng et al., 2018).

As an existing well-established commercial model, APP/PS1 mice have been confirmed well to simulate ALP deficiency in the pathological process of AD. Transmission electron microscopy has shown a large number of autophagic vacuoles containing APP and A β in the brain (Yu et al., 2005; Yu et al., 2004). Previously, our study has confirmed that electroacupuncture plays an essential role in the treatment of Alzheimer's disease by regulating ALP function. Electroacupuncture can effectively regulate LC3 and p62 levels in APP/PS1 mice and improve the fluidity of autophagic flux (Tan et al., 2022). Additionally, EA can also regulate Cathepsin D (CTSD) and Dynein levels to improve transport

and degradation capabilities (Zhang et al., 2022). Furthermore, EA could contribute to the enhancement of cognitive function, reduction of soluble A β_{42} levels in the brain, deceleration of the generation of senile plaques, and even improvement of hippocampal ultrastructure in AD transgenic mice (Wang et al., 2016; Xue et al., 2009; Xue et al., 2011). All of these findings reflect the modulatory effect of electroacupuncture on the aspects of ALP.

Hence, the previous studies have implied that EA could ameliorate ALP impairment in APP/PS1 transgenic mice by upregulating TFEB levels, which might lead to the reduction of A β levels, inhibition of A β pathology, and amelioration of cognitive impairment caused by AD in APP/PS1 transgenic mice. However, the effect and underlying mechanism of EA on the expression of ALP and TFEB need to be further investigated. The findings of the present study will elucidate the mechanism of the effect of EA on ALP of AD mice and promote the broader application of EA in the therapeutic management of AD.

2. Materials and methods

2.1. Experimental animals and grouping

SPF-grade male APP/PS1 transgenic mice ($n = 28$) were obtained from Beijing HFK Bioscience Co., Ltd., with a production license number SCXK(Jing)2019-0008, weighing 26 ± 6 g. SPF-grade male C57BL/6J mice ($n = 14$) were purchased from SPF (Beijing) Biotechnology Co., Ltd., with a production license number: SCXK(Jing)2019-0010, weighing 28 ± 4 g. All animals were eight months old, housed in the Experimental Animal Center of the Beijing University of Chinese Medicine under the circadian of 12-h dark/light, and the ambient temperature and relative humidity were maintained at $23\text{--}26$ °C and 50 ± 2 %, with sterile drinking water and a standard pellet diet available *ad libitum*. After a 7-day adaptation period, the APP/PS1 transgenic mice were randomly divided into the Tg group and the Tg + EA group using a random number table, and the C57BL/6 mice were designated as the WT (wild-type) group, with 14 mice in each group. All protocols were approved by the Animal Ethics Committee, Beijing University of Chinese Medicine, China (Permission number: BUCM-4-2021052406-2041). Every effort was made to minimize the suffering of the mice during the experimental procedure, and all experimental procedures were conducted in accordance with the regulations of the Beijing University of Traditional Chinese Medicine on the management and use of experimental animals.

2.2. Acupuncture intervention

The mice in the WT and Tg groups were immobilized in mouse bags.

For EA intervention, the Tg + EA group was immobilized in the same way as the WT and Tg groups for treatment at Baihui (GV20) and Yongquan (KI1). The selection and position of the acupoints and acupuncture method were based on findings of our previous studies and the group standard T/CAAM 0002-2020, "Names and Locations of Commonly Used Acupuncture Points for Laboratory Animals Part 3: Mice", published on May 15, 2020 by the China Association for Acupuncture and Moxibustion (Fig. 1A). Disposable sterile acupuncture needles (0.25 mm × 13 mm) (Beijing Zhongyan Taihe Medicine Company, Ltd., China) were used.

The treatment was applied every other day and 15 min each time, from days 8 to 49 (6 weeks), with transverse puncturing at bilateral Yongquan (KI1) in a depth of 3–5 mm, Baihui (GV20) in a depth of 2–3 mm. The skin around the acupoints was cleaned with alcohol swabs. The needles in Yongquan (KI1) were connected to an electrical stimulator (Beijing Huawei Medicine Co., Ltd., LH202H, China), and electrical stimulation pulses were applied for 15 min sparse and dense waves (1 mA, 1–50 Hz). Additional stress was strictly avoided during the procedure.

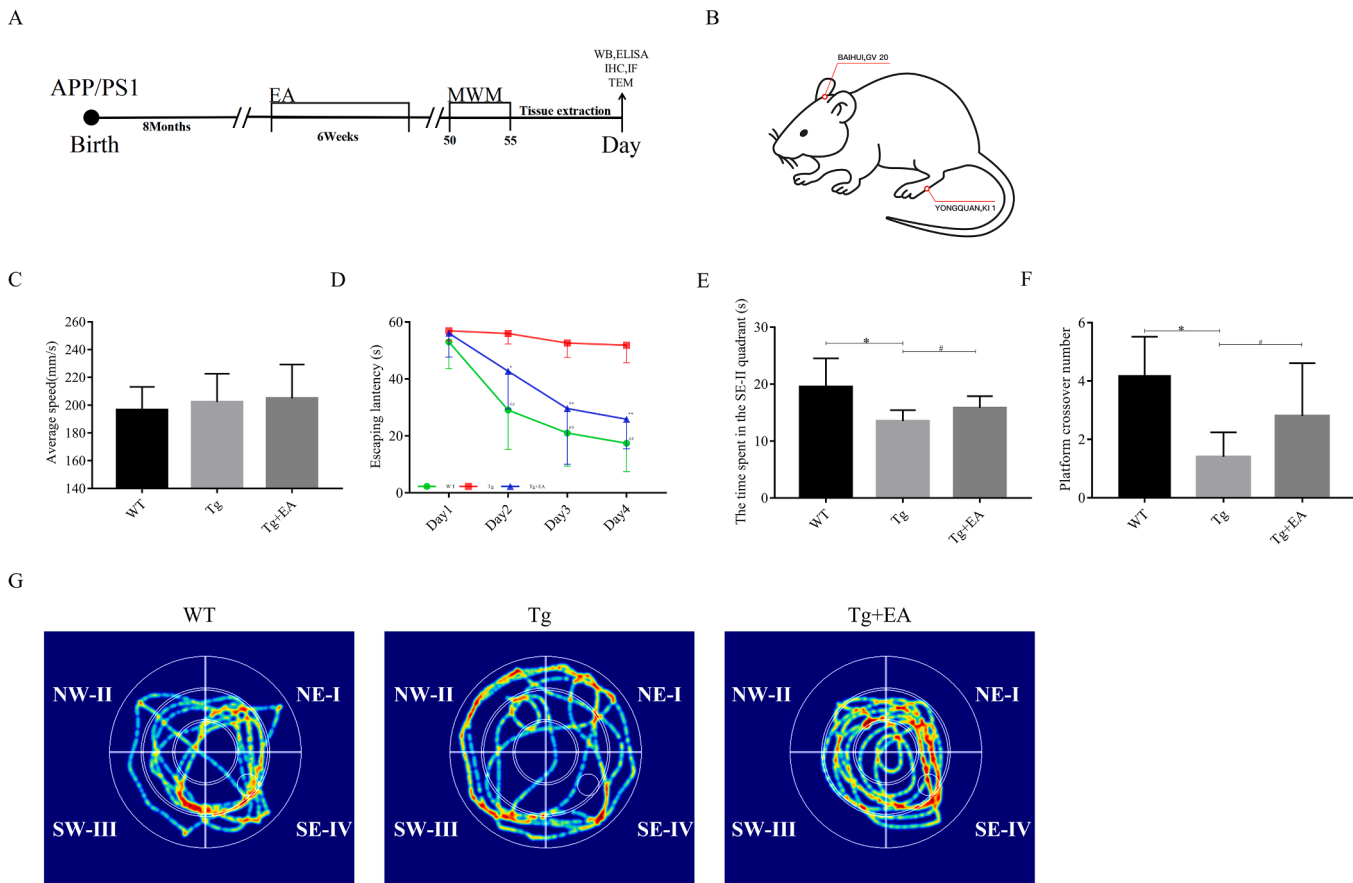


Fig. 1. EA improved spatial learning memory in APP/PS1 mice. (A) Experimental procedures. EA: electroacupuncture; MWM: Morris water maze; TEM: Transmission electron microscopy; IHC: immunohistochemistry; IF: Immunofluorescence; WB: western blot; ELISA: enzyme linked immunosorbent assay. (B) EA demonstrating the position of acupoints GV24 and bilateral KI1, no.2 and no.38 in the image. (C-G) Results of the Morris water maze (MWM) tests in each group ($n = 14$, mean \pm SD). Repeated measures ANOVA with LSD multiple comparison test was used. (C) Comparison between the swimming speed of all groups in the visible platform trial. (D) Quantification of escape latency in each group. * $p < 0.05$, ** $p < 0.01$ vs. wild-type (WT); # $p < 0.05$, ## $p < 0.01$ vs. APP/PS1(Tg). (E, F) Comparison between the platform crossover numbers and the time spent in target quadrant of all groups in the probe trial. (G) Representative moving patterns of mice in each group.

2.3. Morris water maze

Fourteen mice in each group were exposed to the hidden platform trial and the probe trial in turn, from days 50 to 55. All behavioral tests were performed during the animals' light cycle (07:00–19:00). The platform was located in the center of the southeast (SE) quadrant. In the visible platform trial (day 1), the platform was 1 cm above the water. Each mouse was released into the pool facing the wall from all four start locations and had 60 s to search the platform. At the end of each trial, the mouse was placed on the platform or allowed to stay there for 15 s to familiarize the environment. In the hidden platform trial (day 2–5), the platform was hidden 1 cm below the water, and the subsequent procedures were the same as the visible platform trial. The swimming speed in the visible platform trial and the escape latency in the hidden platform trial were collected for subsequent analysis.

The hidden platform trial was performed for four consecutive days. The probe trial (day 6) was after the hidden platform trial; the platform was removed, and each mouse was placed in the pool for 60 s. The starting location farthest from the platform quadrant was used in the probe trial. The platform crossover number and swimming trace were recorded.

2.4. Tissue collection and processing procedures

After 55 days of the experiment, sample collection was conducted on day 56. No mice died during the experiment. On day 56, all the mice were anesthetized by an intraperitoneal injection of pentobarbital (80

mg/kg), and the samples were collected for the laboratory test.

(1) Six mice from each group were chosen for the test of Immunohistochemistry (IHC) and immunofluorescence (IF). Each mouse was anesthetized and perfused transcardially with 0.9 % saline, followed by 4 % paraformaldehyde solution (Coolaber., SL1830, China). The intact brain was removed after perfusion and fixed in 4 % paraformaldehyde solution for 72 h, then dehydrated with 20 % and 30 % sucrose solution in turn. Later, the brain samples were embedded in OCT (Tissue-Tek). The frozen sections of the hippocampal coronary sections behind the optic chiasm were obtained using a cryostat (Leica Corporation, CM1900, Germany) with a thickness of 10 μ m. The sections were then applied for subsequent experiments.

(2) Two mice from each group were subjected to transmission electron microscopy (TEM) analysis. Each mouse was anesthetized and perfused transcardially with PBS solution, followed by a mixture of 2 % paraformaldehyde and 2.5 % glutaraldehyde. The brain was then removed on ice, and small blocks of the CA1 region of the hippocampus were dissected. The tissues were fixed with a solution consisting of 2 % paraformaldehyde and 2.5 % glutaraldehyde and kept at 4 °C for 48 h for subsequent experiments.

(3) Six mice from each group were subjected to western blot and enzyme-linked immunosorbent assay (ELISA) analysis. Each mouse was anesthetized and perfused transcardially with 4 °C PBS solution. The brain was then removed on ice, and the hippocampus tissue was dissected. The dissected tissues (left and right hippocampus) were frozen in liquid nitrogen and stored in a –80 °C freezer for subsequent experiments.

3. Immunohistochemistry

According to the instructions of the IHC kit (Fuzhou Maixin Biotech, Ltd., KIT-9701, and KIT-9706, China), on the first day, the sections were warmed at room temperature for 30 min and then washed three times with PBS. Heat-induced antigen retrieval was performed by incubating the sections in citrate buffer (Fuzhou Maixin Biotech, Ltd., MVS-0066, China) for 15 min, then blocking the sections with goat serum for 10 min after washing. A 100 μ L PBS solution containing anti-amyloid- β 1-16aa primary antibody (1:800, Biolegend, 803001, America) and 0.3 % Triton X-100 (Coolaber., CT11451-100 mL, China) was added to the sections and incubated at 4 °C overnight. On the second day, after washing, the sections were incubated with streptavidin-peroxidase conjugate for 10 min, followed by ready-to-use biotinylated secondary IgG (Fuzhou Maixin Biotech, Ltd., SP KIT-C1, China) for 10 min. 100 μ L DAB solution (Fuzhou Maixin Biotech, Ltd., DAB-0031, China) was added to the sections for 10 min, and the reaction was terminated with water. The sections were dehydrated by immersing in graded ethanol series (70 %–80 %–90 %–95 %–100 %) and immersing in xylene substitute for 20 min. Finally, the sections were mounted with neutral balsam (Beijing Solarbio Science & Technology Co., G8590, China) and photographed.

3.1. Immunofluorescence staining

The first day is the same as immunohistochemistry. Primary antibodies were anti-TFEB antibody (1:300, Bethyl Laboratories, Inc., A303-673A, America), anti-Cathepsin D antibody (1:400, Abcam, ab75852, America), anti-LAMP1 antibody (1:100, Abcam, ab208943, America), anti-amyloid- β 1-16aa primary antibody (1:800, Biolegend, 803001, America). On the second day, after washing, the sections were incubated with Alexa Fluor-conjugated secondary antibodies (1:200, Abcam, ab150077, and ab150115, America) for 2 h in darkness. Ultimately, the sections were stained with a fluorescent mounting medium with DAPI (ZSGB-Bio Co., ZLI-9557, China). Immunofluorescence sections were observed. Fluorescence images were processed using Adobe Photoshop CS (San Jose, CA, USA), analyzed, and quantified using ImageJ (NIH, USA).

3.2. Transmission electron microscopy analysis

Initially, a tissue block of approximately 1 mm × 1 mm × 1 mm was obtained from the CA1 region of the hippocampus. The block was then dehydrated through an acetone gradient and embedded in pure resin. The tissue block was then sectioned and stained with 2 % uranyl acetate and 2 % lead citrate, with a staining time of 5–6 min for lead citrate. This was followed by thorough rinsing with distilled water. Finally, the autophagosomes and autolysosomes were observed with a transmission electron microscope (Hitachi Ltd., H-7560, Japan), and images were taken.

3.3. Enzyme-linked immunosorbent assay analysis

The Human A β 42 Ultrasensitive ELISA Kit (Invitrogen. Inc., KHB3544, Austria) was used to detect soluble A β 42 levels in mouse hippocampus. Procedures were performed according to the instructions provided with the kit. Six samples were collected per group. After the addition of PMSF (Beijing Solarbio Science & Technology Co., A1100, China) and RIPA lysis buffer (Beijing Solarbio Science & Technology Co., R0010, China) (RIPA: PMSF = 100:1), the hippocampus was homogenized and centrifuged at 12,000 rpm for 20 min at 4 °C to collect the supernatant, respectively. The photometric measurements were performed at 450 nm according to the instructions of the manufacturer.

3.4. Western blot analysis

Whole-cell extracts of the hippocampus were obtained with RIPA and PMSF lysis buffer (RIPA: PMSF = 100:1), and nuclear fractions were extracted with the Nuclear and Cytoplasmic Protein Extraction Kit (Beyotime Institute of Biotechnology, P0027, China) according to the manufacturer's instructions. Homogenization and centrifugation were performed as described above. BCA assay (Beijing Solarbio Science & Technology Co., PC0020, China) was used to determine the protein concentration, and the samples were heated at 95 °C for 5 min with a loading buffer. Protein samples were run on 10–12 % Tris-glycine SDS-PAGE gels and transferred to a polyvinylidene difluoride (PVDF) membrane (Millipore, 45PVDF1317-5, America). The membrane was blocked with blocking buffer (NCM Biotech, P30500, China) for 20 min, and incubated with anti-TFEB antibody (1:3000 for whole cell extracts, 1:2000 for the nuclear fractions, Bethyl Laboratories, Inc., A303-673A, America), anti-Cathepsin D antibody (1:10,000, Abcam, ab75852, America), anti-LAMP1 antibody (1:3000, Abcam, ab208943, America), anti-P62/SQSTM1 antibody (1:4000, Proteintech, 18420-1-AP, China), anti-LC3 antibody (1:6000, Proteintech, 14600-1-AP, China), and anti-GAPDH antibody (1:100,000, Proteintech, 60004-1-Ig, China), anti-Histone H3 antibody (1:2000, ImmunoWay Biotechnology, YM3038, America). Primary antibodies were incubated overnight at 4 °C. Respective secondary antibodies (1:5000, Proteintech, SA00001-2, China) (1:5000, ZSGB-Bio Co., ZB-2305, China) were incubated for 60 min at room temperature. Signal intensities were detected by using ECL kits (NCM Biotech, P10100, China) and quantified using ImageJ.

3.5. Statistical analysis

The statistical analysis was performed by SPSS 22.0 (IBM, USA). Data were tested for normal distribution and homogeneity of variance. The group differences in the hidden platform trial are expressed as mean ± standard deviation (mean ± SD) and analyzed by repeated measures analysis of variance. One-way analysis of variance (ANOVA) with the Least-Significant Difference (LSD) post-hoc test was performed to assess between-group differences. The Brown-Forsythe Test or nonparametric tests were used if the variance was not homogeneous or did not conform to a normal distribution. A level of $P < 0.05$ was considered to be significant for analysis.

4. Results

4.1. EA improved the spatial learning and memory of APP/PS1 mice

The results of the Morris water maze test are shown in Fig. 1.

During the visible platform trial, there was no significant difference in the average swimming speed among the three groups ($F = 0.429$, $P > 0.05$), indicating comparable swimming abilities.

In the hidden platform trial, there was a significant difference between the 3 groups. During the test, WT($P < 0.01$) and Tg + EA($P < 0.01$) groups had shown lesser escape latencies than the mice in the Tg group ($F = 31.528$, $P < 0.01$). The Tg group exhibited significantly longer escape latencies compared to the WT group on days 2–4($P < 0.01$). Conversely, the Tg + EA group showed significantly shorter escape latencies compared to the Tg group on days 2–4 ($P < 0.05$), with the most substantial difference observed on day 4 ($P < 0.01$).

During the probe trial, as shown in Fig. 1G, both the WT and Tg + EA groups showed a distinct preference for the target quadrant, indicating preserved spatial memory of the Tg + EA group. In contrast, the Tg group displayed random and aimless swimming patterns, suggesting impaired spatial memory.

In the probe trial, the Tg group spent significantly less time in the SE-IV quadrant ($F = 10.256$, $P < 0.01$) and exhibited a less platform crossover numbers ($F = 8.331$, $P < 0.01$) compared to both the WT($P < 0.01$ and $P < 0.01$) and Tg + EA($P < 0.05$ and $P < 0.01$) groups.

These findings highlight that EA intervention can effectively improve the spatial learning and memory ability of Tg mice.

4.2. EA inhibited A β deposition in the hippocampus of APP/PS1 mice

The results of the immunohistochemical method of A β in the hippocampal region are shown in Fig. 2A.

In the WT group, there was no positive expression of A β and senile plaques in the visual field. In the Tg group, there was an obvious brown positive expression of A β in the cytoplasm of neurons in the hippocampal pyramidal layer (stratum pyramidale), and a large number of more obvious nucleated dense plaques were seen in the hippocampal

area, i.e., typical senile plaques. The central core was densely and uniformly stained, surrounded by a radially spreading corolla. In the Tg + EA group, the positive expression of senile plaques and the positive expression of A β such as senile plaques and neurons in the pyramidal layer (stratum pyramidale), as well as in the radial layer (stratum radiatum) and dentate gyrus regions, was reduced.

4.3. EA reduced soluble A β_{42} level in the hippocampus of the APP/PS1 mice

The ELISA results of the hippocampal tissue are shown in Fig. 2. Significant differences were observed in the levels of soluble A β_{42}

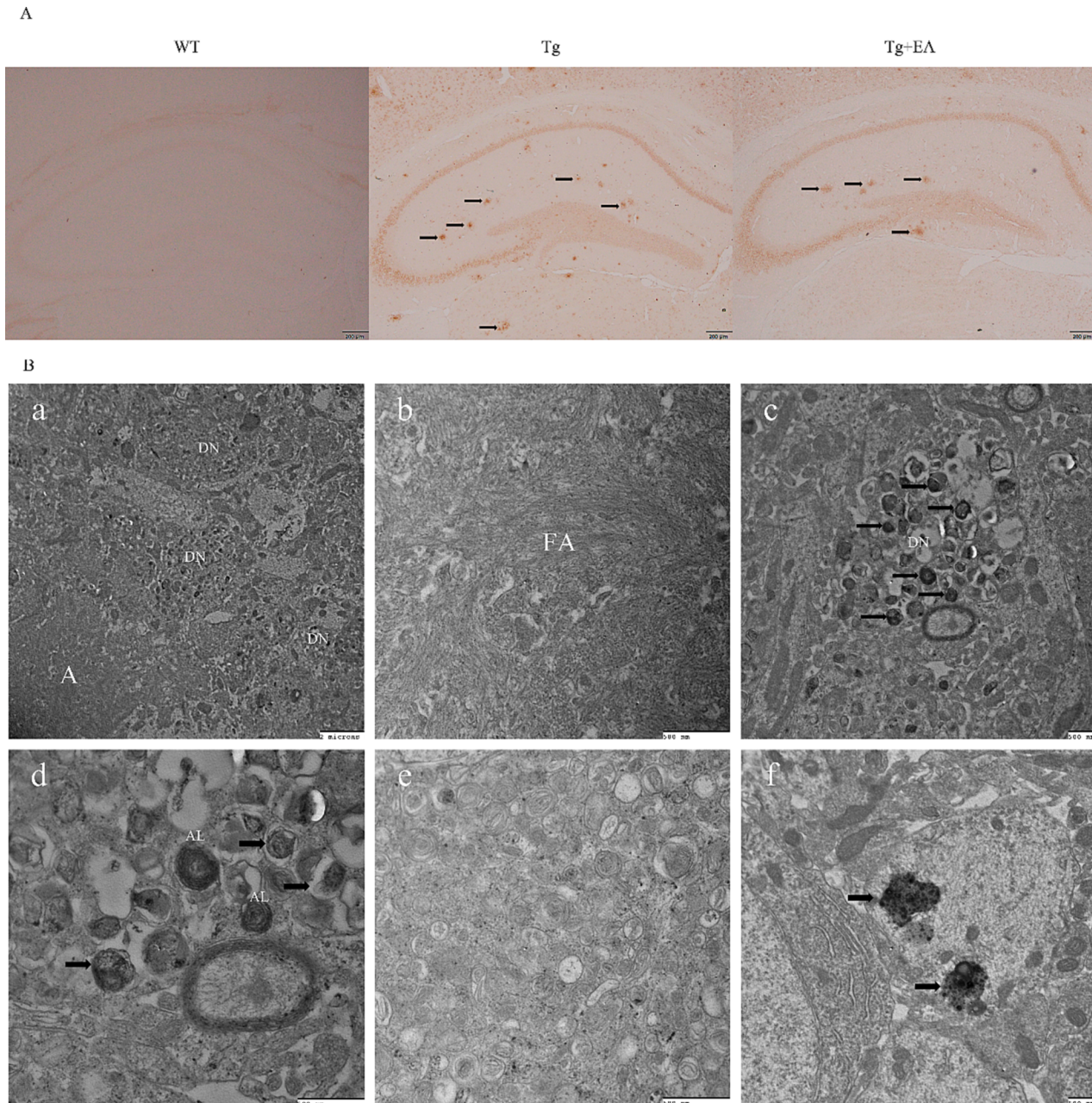


Fig. 2. A β and ALP-dysfunction pathology in APP/PS1 mice hippocampus. (A) Immunohistochemistry for A β in each group. (B) Transmission electron microscopy images of the hippocampus of APP/PS1 mice. Figure a magnification 8000 \times , Figure b, d, e magnification 50000 \times , Figure c, f magnification 20000 \times . a. Panoramic view of amyloid- β pathology, which contains dense amyloid core (A) surrounded by dystrophic neurites (DN). b. Compact fibrillar amyloid (FA) in amyloid plaque core. c, d. Ultrastructure images of dystrophic neurites, containing abundant electrodense degradative autophagic vesicles (arrows, Fig. c, d), usually present around compact amyloid core. e. Dystrophic neurites with low electrodense view, being gradually eroded by amyloid- β , may develop into senile plaques. f. Autolysosomes (multivesicular bodies, arrows) in the cytoplasm of neuron, may failed in acidification.

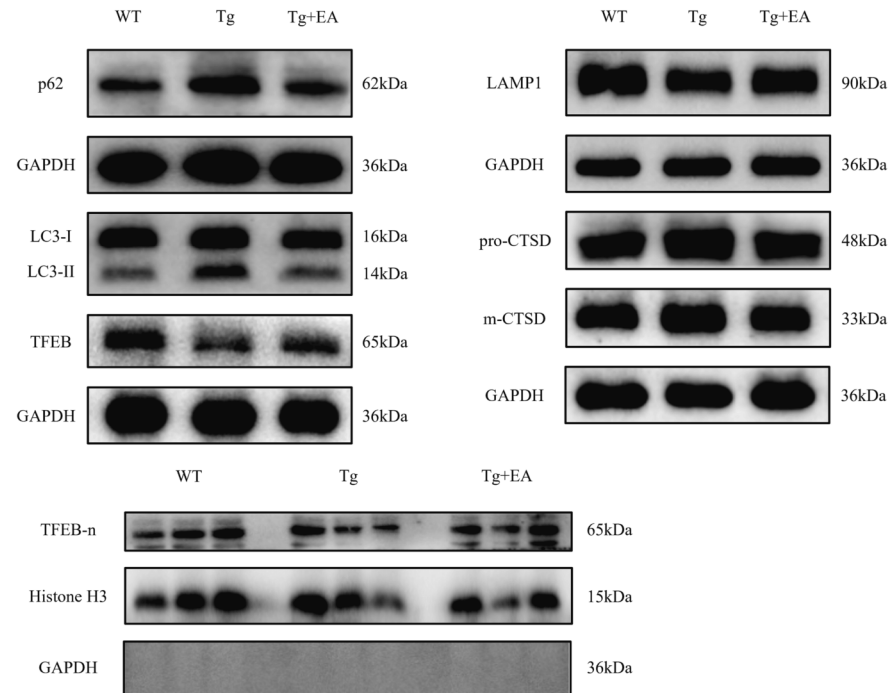
among the groups, with statistical significance ($F = 69.060$, $P < 0.01$). In the WT group, minimal expression of human-derived A β was detected. Conversely, the Tg group displayed a significant increase in soluble A β_{42} levels in the hippocampus compared to the WT group ($P < 0.01$). Importantly, the Tg + EA group exhibited a notable decrease in soluble A β_{42} levels in the hippocampus compared to the Tg group ($P < 0.01$), indicating that EA intervention can effectively reduce the burden of soluble A β_{42} in the hippocampus of APP/PS1 mice.

5. Ultrastructure characteristics of hippocampus in APP/PS1 mice

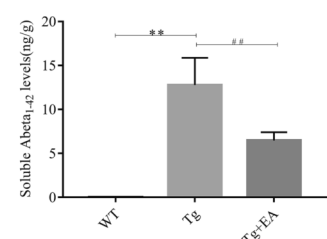
The results of the immunohistochemical method of A β in the hippocampal region are shown in Fig. 2B, which shows the hippocampal ultrastructure of APP/PS1 transgenic AD mice.

The ultrastructure of the hippocampus in APP/PS1 mice was examined using transmission electron microscopy, revealing a notable abundance of senile plaques. Upon closer examination, distinct fibrillar amyloid were observed within the senile plaques. Surrounding the senile plaques, numerous dystrophic neurites of varying sizes were present,

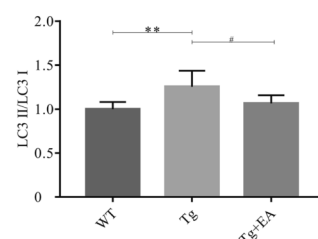
A



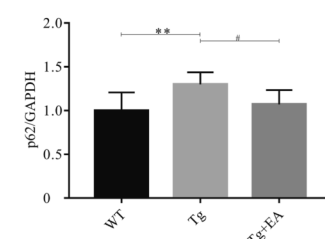
B



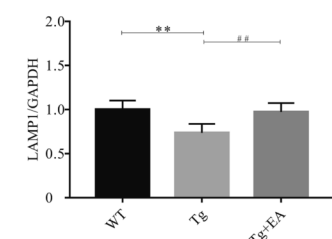
C



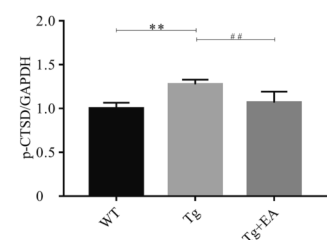
D



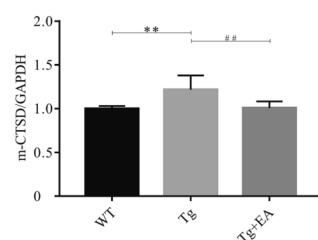
E



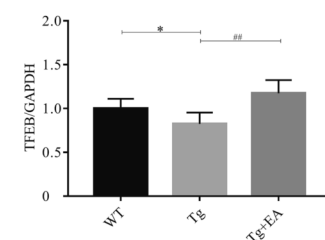
F



G



H



I

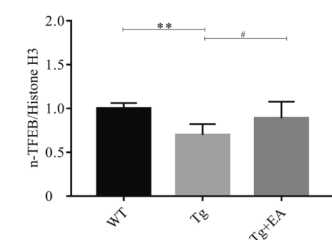


Fig. 3. EA increased TFEB expression and ameliorated autophagy-lysosomal pathway dysregulation in APP/PS1 mice hippocampus. (A) Representative western blots showed the levels of ALP markers (LC3, p62, LAMP1, CTSD), TFEB and n-TFEB of mice hippocampus. (B) Effect of EA on the level of the soluble A β ₄₂ level of hippocampus in each group ($n = 6$, mean \pm SD), analyzed by One-way ANOVA followed by LSD's post-hoc test. * $p < 0.05$, ** $p < 0.01$ vs. wild-type (WT); # $p < 0.05$, ## $p < 0.01$ vs. APP/PS1(Tg). (C-I) Data were quantified ($n = 6$, mean \pm SD) by image J and analyzed by One-way ANOVA followed by LSD's post-hoc test. * $p < 0.05$, ** $p < 0.01$ vs. wild-type (WT); # $p < 0.05$, ## $p < 0.01$ vs. APP/PS1(Tg).

and further magnification revealed a substantial presence of autophagic vacuoles, including electron-dense degradative autophagic vacuoles, indicating dysfunction of the autophagic flux. Additionally, evidence of autolysosomes with impaired acidification was observed within the neuronal cytoplasm. Moreover, the observation of dystrophic neurites infiltrated with A β or the development of new senile plaques was noted.

These findings collectively indicate a significant presence of A β pathology and impaired ALP in the hippocampus of APP/PS1 mice.

5.1. EA enhanced autophagic flux in APP/PS1 mice

As shown in Fig. 3, there was a significant difference in the ratio of LC3 II/LC3 I, an autophagy-lysosomal pathway (ALP) marker, among the groups ($F = 6.58$, $P < 0.01$). Compared to the WT group, the Tg group exhibited a significant increase in the LC3 II/LC3 I ratio ($P < 0.01$). Furthermore, compared to the Tg group, the Tg + EA group showed a decreased LC3 II/LC3 I ratio ($P < 0.05$).

A significant difference was also observed in the relative expression

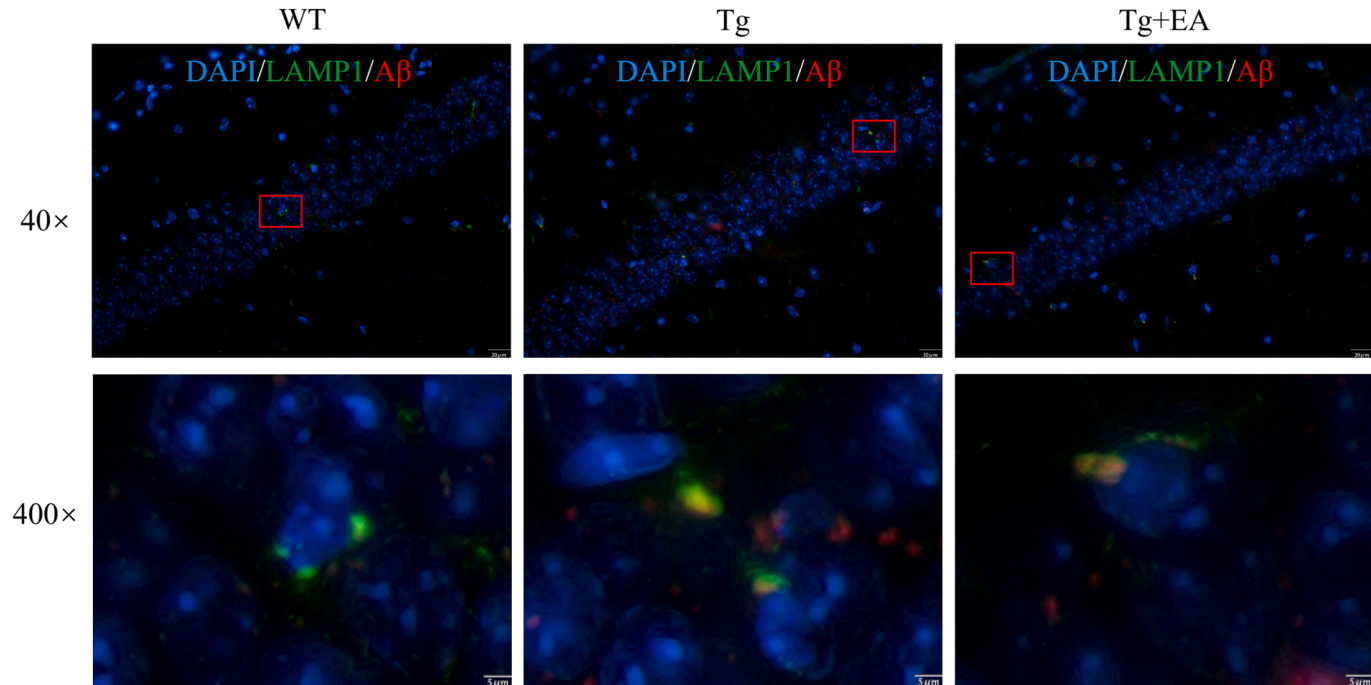
levels of p62, another ALP marker, among the groups ($F = 4.934$, $P < 0.05$). The Tg group showed a significant increase in the relative expression of p62 compared to the WT group ($P < 0.01$). In contrast, the Tg + EA group showed decreased relative expression levels of p62 compared to the Tg group ($P < 0.05$).

The elevated LC3-II/LC3-I ratio and p62 levels in the Tg group, compared to the WT group, suggested the presence of ALP impairment disrupted autophagic flux and accumulation of autophagic vesicles in the hippocampus of APP/PS1 mice. The results in the Tg + EA group demonstrated a significant reduction compared to the Tg group, indicating that EA intervention relieved the ALP function.

5.2. EA improved lysosomal formation in APP/PS1 mice

The relative expression levels of LAMP1, a lysosomal marker, also showed significant differences among the groups ($F = 12.028$, $P < 0.01$). The Tg group exhibited a significant decrease in the relative expression of LAMP1 compared to the WT group ($P < 0.01$). In contrast, the Tg +

A



B

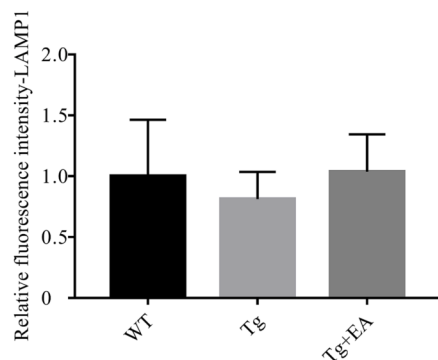


Fig. 4. EA promoted the formation of lysosomes in APP/PS1 mice hippocampus. (A) Representative fluorescent images of LAMP1(green) and A β (red) in hippocampus of mice from WT, Tg and Tg + EA groups. Original magnification: 40 \times , scale bar: 20 μ m. Corresponding zoom-in images (scale bar: 5 μ m) were processed using ImageJ to demonstrate the colocalization. (B) The relative fluorescence intensity of LAMP1 in hippocampus was quantified ($n = 6$, mean \pm SD) by image J and analyzed by One-way ANOVA followed by LSD's post-hoc test. * $p < 0.05$, ** $p < 0.01$ vs. wild-type (WT); # $p < 0.05$, ## $p < 0.01$ vs. APP/PS1(Tg). (For interpretation of the references to colour in this figure legend, the reader is referred to the web version of this article.)

EA group showed an increased relative expression levels of LAMP1 compared to the Tg group ($P < 0.01$).

By immunofluorescence imaging, the positive expression of LAMP1 was localized in the cytoplasm (Fig. 4). The relative fluorescence intensity of LAMP1 was higher in both the WT and Tg + EA groups compared to the Tg group, although the difference was not statistically significant ($F = 0.725$, $P > 0.05$).

These findings have indicated that the lysosomal function was impaired in APP/PS1 mice, resulting in a reduced number of lysosomes compared to WT mice. However, EA intervention contributed to an increase in lysosome numbers and improvement in lysosomal activity.

6. EA modulated lysosome degradation in APP/PS1 mice

Significant differences were observed in the relative expression levels of pro-CTSD, a lysosomal marker, among the groups ($F = 16.003$, $P < 0.01$). The Tg group showed a significant increase in the relative expression of pro-CTSD compared to the WT group ($P < 0.01$). In contrast, the Tg + EA group showed a significant decreased relative expression level of pro-CTSD compared to the Tg group ($P < 0.01$).

Similarly, significant differences were observed in the relative

expression levels of m-CTSD, another lysosomal marker, among the groups ($F = 8.273$, $P < 0.01$). The Tg group exhibited a significant increase in the relative expression of m-CTSD compared to the WT group ($P < 0.01$). However, the Tg + EA group showed a significant decreased relative expression level of pro-CTS compared to the Tg group ($P < 0.01$).

The 48 kDa pro-CTSD primarily localized to endosomes and amphisomes, while the 33 kDa m-CTSD mainly resided in lysosomes and played a role in the degradation process of A β . The elevated levels of CTSD in the Tg group compared to the WT group suggested the accumulation and impaired degradation of autolysosomes and amphisomes. However, in the Tg + EA group, the levels of CTSD decreased, indicating that with improved autophagic flux, the activity of lysosomal function was also enhanced.

By immunofluorescence imaging, positive expression of CTSD localized around nucleus was found (Fig. 5). The relative fluorescence intensity of CTSD was lower in both the WT and Tg + EA groups compared to the Tg group, but the difference was not statistically significant ($F = 10.286$, $P > 0.05$). Additionally, the proportion of yellow fluorescence (indicating co-localization of CTSD and A β) ($F = 10.058$, $P < 0.01$) was significantly lower in the WT ($P < 0.01$) and Tg + EA ($P <$

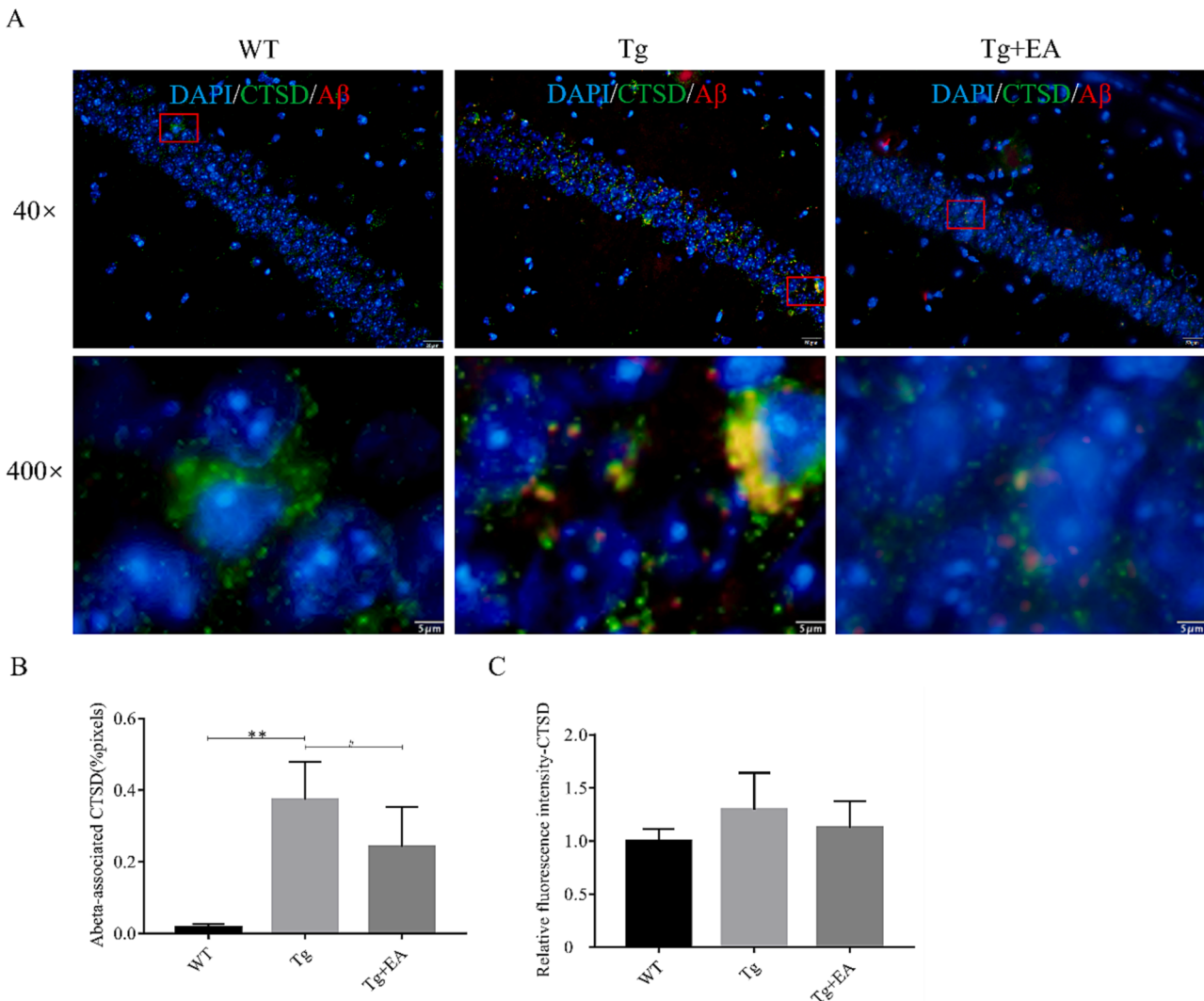


Fig. 5. EA promoted the degradation of autolysosomes in APP/PS1 mice hippocampus. (A) Representative fluorescent images of CTSD (green) and A β (red) in hippocampus of mice from WT, Tg and Tg + EA groups. Original magnification: 40 \times , scale bar: 20 μ m. Corresponding zoom-in images (scale bar: 5 μ m) were processed using ImageJ to demonstrate the colocalization. (B) The relative fluorescence intensity of CTSD and the %pixels of A β associated CTSD in hippocampus was quantified ($n = 6$, mean \pm SD) by image J and analyzed by one-way ANOVA followed by LSD's post-hoc test. * $p < 0.05$, ** $p < 0.01$ vs. wild-type (WT); # $p < 0.05$, ## $p < 0.01$ vs. APP/PS1(Tg). (For interpretation of the references to colour in this figure legend, the reader is referred to the web version of this article.)

0.05) groups compared to the Tg group.

The reduced proportion of yellow fluorescence in the Tg + EA group suggested that EA intervention ameliorated the accumulation of degradative vesicles and enhanced neuronal degradation function. These results collectively indicate the presence of an accumulation of degradative vesicles containing A β in the Tg group, with impaired degradation of A β , supporting the previous western blot results.

6.1. EA upregulated TFEB function in hippocampus of APP/PS1 mice

The relative expression levels of TFEB ($F = 10.599$, $P < 0.01$) and n-TFEB ($F = 10.036$, $P < 0.05$) showed significant differences among the groups, as depicted in Fig. 3. In comparison to the WT group, the Tg group exhibited significantly lower levels of TFEB ($P < 0.05$) and n-TFEB ($P < 0.01$). However, EA intervention resulted in a significant increase in the levels of TFEB ($P < 0.01$) and n-TFEB ($P < 0.05$) in APP/PS1 mice when compared to the Tg group. The relative fluorescence intensity of TFEB was higher in both the WT ($P < 0.01$) and Tg + EA ($P < 0.01$) groups compared to the Tg group, and the difference was statistically

significant ($F = 12.651$, $P < 0.01$) (Fig. 6).

TFEB is predominantly distributed in the cytoplasm (Fig. 6A) and requires dephosphorylation to undergo nuclear translocation and activation. TFEB promotes the transcription of genes related to the autophagy-lysosomal pathway (ALP), while its own gene transcription is also regulated by TFEB. Therefore, the aforementioned findings indicate that the expression and nuclear translocation levels of TFEB are down-regulated in the Tg group, suggesting TFEB dysfunction. On the other hand, electroacupuncture may modulate the functional status of ALP in APP/PS1 transgenic mice by influencing the nuclear translocation of TFEB.

7. Discussion

Acupuncture has long been used in Asia to treat AD, but the underlying mechanisms are not well understood. As an advanced acupuncture technique, electroacupuncture utilizes electrical stimulation to enhance the effects of acupuncture. Existing research has suggested that acupuncture may improve cognitive function through various

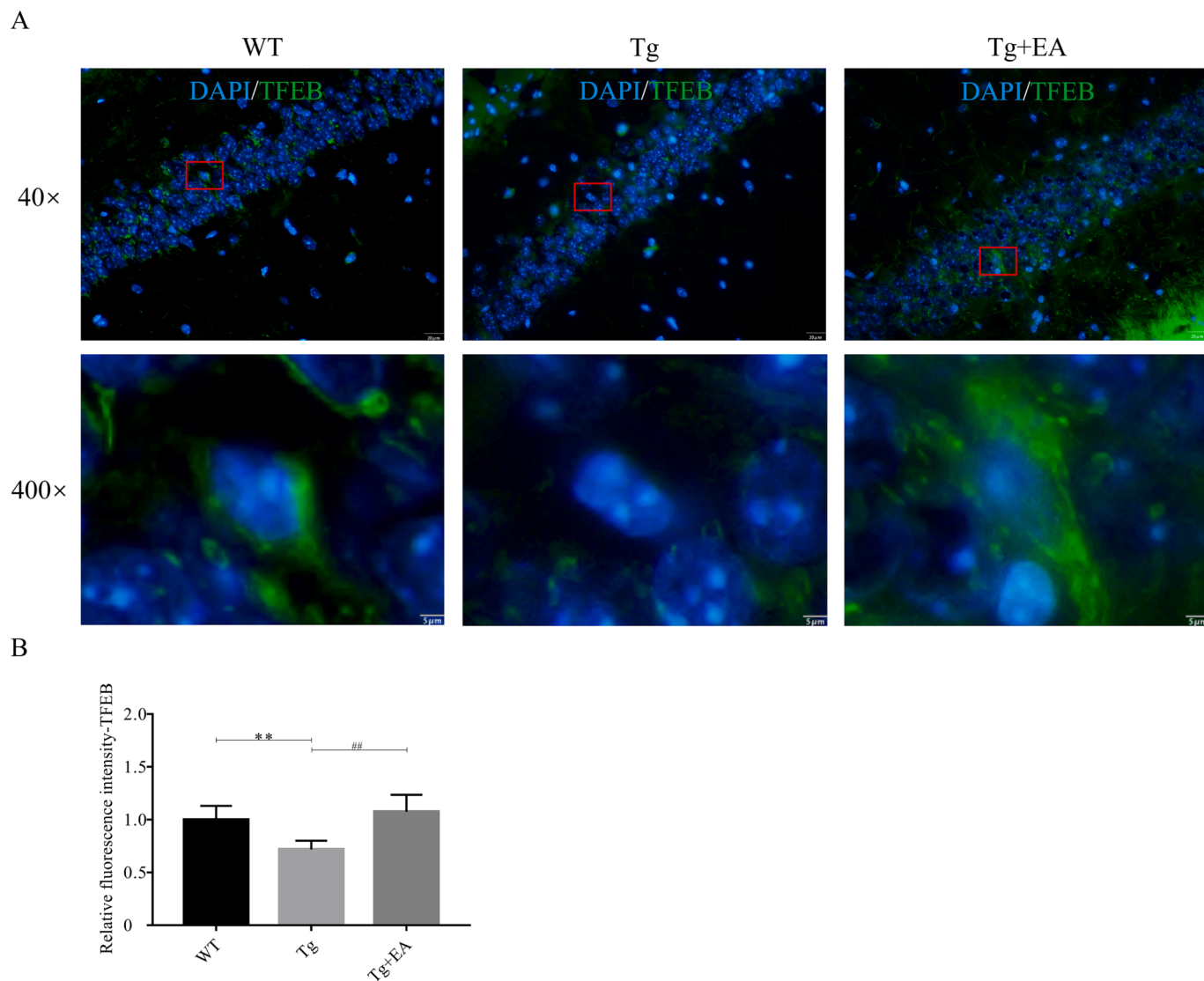


Fig. 6. EA increased the expression of TFEB in APP/PS1 mice hippocampus. (A) Representative fluorescent images of TFEB (green) in the hippocampus of mice from WT, Tg and Tg + EA groups. Original magnification: 40 \times , scale bar: 20 μ m. Corresponding zoom-in images (scale bar: 5 μ m) were processed using ImageJ to observe the details. (B) The relative fluorescence intensity of TFEB in hippocampus was quantified ($n = 6$, mean \pm SD) by image J and analyzed by One-way ANOVA followed by LSD's post-hoc test. * $p < 0.05$, ** $p < 0.01$ vs. wild-type (WT); # $p < 0.05$, ## $p < 0.01$ vs. APP/PS1(Tg). (For interpretation of the references to colour in this figure legend, the reader is referred to the web version of this article.)

mechanisms, including reducing tau phosphorylation levels (Zhang et al., 2017), modulating neurotransmitters (Yun et al., 2017), and promoting neurogenesis (Zhao et al., 2019). These findings underscore the broad scope and multiple targets of EA and highlight its multifaceted effects.

The Morris water maze is a widely recognized and extensively used behavioral method to investigate spatial learning and memory in animals following hippocampal damage. It serves as a valuable tool for assessing cognitive dysfunction in animal models of Alzheimer's disease (Tomás Pereira et al., 2015). The results of the visible platform test revealed no significant difference in swimming speed among the groups, indicating similar motor abilities across the experimental groups. In the hidden platform test, the Tg group exhibited a significantly longer escape latency on days 2–4 compared to the WT group, indicating impaired spatial learning and memory abilities in the APP/PS1 mice. Furthermore, during the probe trial, the Tg group showed significantly reduced time spent in the SE-IV quadrant and a smaller number of platform crossovers compared to the WT group. These findings suggested a clear decline in spatial learning and memory in the APP/PS1 mice, closely resembling the cognitive impairment of Alzheimer's disease (De Felice and Munoz, 2016). Importantly, the application of EA intervention significantly ameliorated the observed changes, demonstrating its effectiveness in improving the cognitive abilities of APP/PS1 mice. These results aligned with our previous study and further support the beneficial effects of EA in the treatment of AD.

Based on the results of A β immunohistochemistry and ELISA in the hippocampus, it indicated that EA effectively reduced soluble A β_{42} levels in the hippocampus of APP/PS1 mice and inhibited the formation of senile plaques. This demonstrated the ameliorative effect of EA on A β pathology.

A β pathology, as the primary pathological alteration in AD, plays a critical role in the stages of AD progression. Emerging evidence has suggested that neurons are the primary source of A β in the brain. With secretion, it enters the intercellular space, while astrocytes and microglia also produce small amounts of A β (Niederst et al., 2015). Recent studies have highlighted the selective generation of A β in dysfunctional acidified autolysosomes (Lee and Nixon, 2022). Our previous investigations have shown that EA modulates the initiation of autophagy, autophagosome transport, and lysosomal degradation processes (Tan et al., 2022; Zhang et al., 2022; Wang et al., 2016; Xue et al., 2009; Xue et al., 2011). In addition, accumulating research have verified the importance of TFEB as a key regulator of the ALP (Settembre et al., 2011). Thus, we postulated that EA improves cognitive function in AD model mice by regulating TFEB function, thereby ameliorating ALP deficiency in AD, enhancing A β clearance, attenuating A β production, and ultimately inhibiting the progression of A β pathology while improving spatial learning memory. The results have confirmed the positive modulatory effect of EA on cognitive function and underscore the feasibility of the EA intervention protocol used in this study. The technical details of the acupoints, manipulations, and treatment protocols used in this research may provide valuable insights for future investigations.

The western blot analysis revealed that the Tg group exhibited significantly higher levels of the LC3-II/LC3-I ratio and p62 compared to the WT group. Additionally, TEM examination demonstrated the presence of numerous dystrophic neurites surrounding the senile plaques in the Tg group, indicating the accumulation of autophagic vesicles and impaired autophagic flux. Furthermore, the Tg group exhibited significantly lower levels of TFEB, n-TFEB, and the lysosomal marker LAMP1, along with significantly higher levels of pro- and m-CTSD, when compared to the WT group. These findings suggested that the reduced TFEB levels, coupled with the inhibition and dysfunction of TFEB's nuclear translocation, led to a decrease in lysosome numbers and an accumulation of autophagic vesicles containing hydrolases. These results are consistent with the previously reported pathological features of impaired ALP in AD patients (Lee and Nixon, 2022; Bordi et al., 2016; Lie et al., 2021).

Notably, the Tg + EA group showed significantly lower levels of the LC3-II/LC3-I ratio and p62 compared to the Tg group, indicating an improvement in autophagic flux deficiency and the accumulation of autophagic vesicles. These findings suggested that EA intervention can upregulate TFEB levels and promote TFEB's nuclear translocation, thus ameliorating ALP dysfunction in APP/PS1 mice, which in turn reduces A β levels, inhibits the development of A β pathology and ameliorates cognitive impairment associated with AD.

An increasing number of studies have provided evidence that acupuncture can modulate the function and activity of the ALP to facilitate the degradation of proteins prone to aggregation. This effect can decelerate the accumulation of abnormal proteins and disease progression, thereby exerting therapeutic effects on various neurodegenerative diseases, including AD and PD (Parkinson's disease) (Guo et al., 2016; Tian et al., 2016; Wang et al., 2018; Zheng et al., 2021). These findings provide new possibilities and broader avenues for future research in this field.

However, it is important to acknowledge that there are still limitations in the experimental design of the present study. Future studies can focus on optimizing the experimental design to address these limitations. This may include increasing the sample size to enhance statistical power and reliability of the results. Additionally, the inclusion of control groups, such as sham acupuncture, positive drug treatment, and inhibitors, can provide a more comprehensive understanding of the effects of acupuncture in comparison to other interventions. By refining the experimental design, we can obtain more robust and reliable data to further elucidate the potential benefits of acupuncture in the treatment of neurodegenerative diseases.

In conclusion, this study provides further evidence that EA can improve cognitive function in APP/PS1 mice, and the effects of EA may be mediated through modulation of hippocampal ALP.

Notably, the present study preliminarily highlights the role of EA in alleviating cognitive deficits induced by A β pathology and ALP deficits in the APP/PS1 model, providing new experimental evidence to support the treatment of AD.

The present study has shown that EA effectively ameliorates ALP dysfunction and abnormal TFEB activity in APP/PS1 mice, thereby inhibiting the progression of A β pathology. The direct regulation of ALP by TFEB might play a critical role in the beneficial modulation of cognitive function and A β pathology by EA. Therefore, the beneficial effects of EA on cognitive function and A β pathology are likely achieved through the regulation of TFEB activity.

Ethical approval and consent to participate

All animal experiments and protocols complied with international animal experimental ethics and requirements, and were approved by the Animal Ethics Committee, Beijing University of Chinese Medicine, China (Permit No. BUCM-4-2021052406-2041).

Funding

The authors' work reported here was supported by grants from the Beijing Municipal Natural Science Foundation Grants Program (No. 7202117).

10. Authors' contributions

Weiguo Xue designed research and fund acquisition. Haotian Chen and Xiaokun Yang performed research. Yushan Gao and Mengwei Guo provided technical assistance for the research. Chenlu Li, Yunxiang Tan, and Yang Zhang provided experimental assistance. Haotian Chen and Xiaokun Yang performed statistical analysis and wrote the paper. Huili Jiang provided guidance in writing and review. Haotian Chen and Xiaokun Yang share co-first author.

Declaration of Competing Interest

The authors declare that they have no known competing financial interests or personal relationships that could have appeared to influence the work reported in this paper.

Data availability

Data will be made available on request.

Appendix A. Supplementary data

Supplementary data to this article can be found online at <https://doi.org/10.1016/j.brainres.2023.148683>.

References

- [1] 2022 Alzheimer's disease facts and figures, *Alzheimer's & Dementia*, 18 (2022) 700–789. <https://doi.org/10.1002/alz.12638>.
- Bao, J., Zheng, L., Zhang, Q., Li, X., Zhang, X., Li, Z., Bai, X., Zhang, Z., Huo, W., Zhao, X., Shang, S., Wang, Q., Zhang, C., Ji, J., 2016. Deacetylation of TFEB promotes fibrillar Abeta degradation by upregulating lysosomal biogenesis in microglia. *Protein Cell* 7, 417–433. <https://doi.org/10.1007/s13238-016-0269-2>.
- Bordi, M., Berg, M.J., Mohan, P.S., Peterhoff, C.M., Alldred, M.J., Che, S., Ginsberg, S.D., Nixon, R.A., 2016. Autophagy flux in CA1 neurons of Alzheimer hippocampus: increased induction overburdens failing lysosomes to propel neuritic dystrophy. *Autophagy* 12, 2467–2483. <https://doi.org/10.1080/15548627.2016.1239003>.
- Caccamo, A., Majumder, S., Richardson, A., Strong, R., Oddo, S., 2010. Molecular interplay between mammalian target of rapamycin (mTOR), amyloid- β , and Tau: effects on cognitive impairments. *J. Biol. Chem.* 285, 13107–13120. <https://doi.org/10.1074/jbc.M110.100420>.
- Caو, Y., Zhang, L., Wang, J., Du, S., Xiao, L., Tu, J., Liu, C., 2016. Mechanisms of acupuncture effect on Alzheimer's disease in animal-based researches. *Curr. Top. Med. Chem.* 16, 574. <https://doi.org/10.2174/1568026615666150813144942>.
- Cortes, C.J., La Spada, A.R., 2019. TFEB dysregulation as a driver of autophagy dysfunction in neurodegenerative disease: molecular mechanisms, cellular processes, and emerging therapeutic opportunities. *Neurobiol. Dis.* 122, 83–93. <https://doi.org/10.1016/j.nbd.2018.05.012>.
- De Felice, F.G., Munoz, D.P., 2016. Opportunities and challenges in developing relevant animal models for Alzheimer's disease. *Ageing Res. Rev.* 26, 112–114. <https://doi.org/10.1016/j.arr.2016.01.006>.
- Du, K., Yang, S., Wang, J., Zhu, G., Junli, Z., Zhao, J., 2022. Acupuncture interventions for Alzheimer's disease and vascular cognitive disorders: a review of mechanisms. *Oxid. Med. Cell. Longev.* 2022, 1–18. <https://doi.org/10.1155/2022/6080282>.
- Eimer, W.A., Vassar, R., 2013. Neuron loss in the 5XFAD mouse model of Alzheimer's disease correlates with intraneuronal Abeta42 accumulation and Caspase-3 activation. *Mol. Neurodegener.* 8, 2. <https://doi.org/10.1186/1750-1326-8-2>.
- Gauthier, S., Webster, C., Servaes, S., AMorais, J., Rosa-Neto, P., World Alzheimer Report 2022: Life after diagnosis: Navigating treatment, care and support, 2022.
- Guo, H.D., Zhu, J., Tian, J.X., Shao, S.J., Xu, Y.W., Mou, F.F., Han, X.J., Yu, Z.H., Chen, J., L., Zhang, D.Y., Zhang, L.S., Cui, G.H., 2016. Electroacupuncture improves memory and protects neurons by regulation of the autophagy pathway in a rat model of Alzheimer's disease. *Acupunct. Med.* 34, 449–456. <https://doi.org/10.1136/acupmed-2015-010894>.
- Jia, Y., Zhang, X., Yu, J., Han, J., Yu, T., Shi, J., Zhao, L., Nie, K., 2017. Acupuncture for patients with mild to moderate Alzheimer's disease: a randomized controlled trial. *Bmc Complement. Altern. M* 17, 556. <https://doi.org/10.1186/s12906-017-2064-x>.
- Karran, E., Mercken, M., Strooper, B.D., 2011. The amyloid cascade hypothesis for Alzheimer's disease: an appraisal for the development of therapeutics. *Nat. Rev. Drug Discov.* 10, 698–712. <https://doi.org/10.1038/nrd3505>.
- Lane, C.A., Hardy, J., Schott, J.M., 2018. Alzheimer's disease. *Eur. J. Neurol.* 25, 59–70. <https://doi.org/10.1111/ene.13439>.
- Lee, J., Nixon, R.A., 2022. Autolysosomal acidification failure as a primary driver of Alzheimer disease pathogenesis. *Autophagy* 18, 2763–2764. <https://doi.org/10.1080/15548627.2022.2110729>.
- Liang, J., Jia, J., 2014. Dysfunctional autophagy in Alzheimer's disease: pathogenic roles and therapeutic implications. *Neurosci. Bull.* 30, 308–316. <https://doi.org/10.1007/s12264-013-1418-8>.
- Lei, P.P.Y., Yang, D., Stavrides, P., Goulbourne, C.N., Zheng, P., Mohan, P.S., Cataldo, A. M., Nixon, R.A., 2021. Post-Golgi carriers, not lysosomes, confer lysosomal properties to pre-degradative organelles in normal and dystrophic axons. *Cell Rep.* 35, 109034 <https://doi.org/10.1016/j.celrep.2021.109034>.
- Niederst, E.D., Reyna, S.M., Goldstein, L.S.B., Forscher, P., 2015. Axonal amyloid precursor protein and its fragments undergo somatodendritic endocytosis and processing. *Mol. Biol. Cell* 26, 205–217. <https://doi.org/10.1091/mbc.E14-06-1049>.
- Nixon, R.A., 2007. Autophagy, amyloidogenesis and Alzheimer disease. *J. Cell Sci.* 120, 4081–4091. <https://doi.org/10.1242/jcs.019265>.
- Nixon, R.A., Yang, D., 2011. Autophagy failure in Alzheimer's disease—locating the primary defect. *Neurobiol. Dis.* 43, 38–45. <https://doi.org/10.1016/j.nbd.2011.01.021>.
- Rahman, M.A., Rahman, M.S., Rahman, M.H., Rasheduzzaman, M., Mamun-Or-Rashid, A., Uddin, M.J., Rahman, M.R., Hwang, H., Pang, M., Rhim, H., 2021. Modulatory effects of autophagy on APP processing as a potential treatment target for Alzheimer's Disease. *Biomedicines* 9, 5. <https://doi.org/10.3390/biomedicines9010005>.
- Reddy, K., Cusack, C.L., Nnah, I.C., Khayati, K., Saqena, C., Huynh, T.B., Noggle, S.A., Ballabio, A., Dobrowski, R., 2016. Dysregulation of nutrient sensing and CLEARance in presenilin deficiency. *Cell Rep.* 14, 2166–2179. <https://doi.org/10.1016/j.celrep.2016.02.006>.
- Sardiello, M., Palmieri, M., di Ronza, A., Medina, D.L., Valenza, M., Gennarino, V.A., Di Malta, C., Donaudy, F., Embrione, V., Polischuk, R.S., Banfi, S., Parenti, G., Cattaneo, E., Ballabio, A., 2009. A gene network regulating lysosomal biogenesis and function. *Science (Am. Assoc. Advance. Sci.)* 325, 473–477. <https://doi.org/10.1126/science.1174447>.
- Settembre, C., Di Malta, C., Polito, V.A., Arencibia, M.G., Vetrini, F., Erdin, S., Erdin, S.U., Huynh, T., Medina, D., Colella, P., Sardiello, M., Rubinsztein, D.C., Ballabio, A., 2011. TFEB links autophagy to lysosomal biogenesis. *Science* 332, 1429–1433. <https://doi.org/10.1126/science.1204592>.
- Tan, Y.X., Zhang, Y., Gao, Y.S., Pei, Y.N., Yang, X.K., Li, C.L., Xue, W.G., 2022. Effects of electroacupuncture on the expression of beta-amyloid and autophagy-related proteins in hippocampal cells of mice with Alzheimer's disease [Chinese]. *Zhen Ci Yan Jiu* 47, 1048–1053. <https://doi.org/10.13702/j.1000-0607.20211232>.
- Tian, T., Sun, Y., Wu, H., Pei, J., Zhang, J., Zhang, Y., Wang, L., Li, B., Wang, L., Shi, J., Hu, J., Fan, C., 2016. Acupuncture promotes mTOR-independent autophagic clearance of aggregation-prone proteins in mouse brain. *Sci. Rep.-Uk* 6, 19714. <https://doi.org/10.1038/srep19714>.
- Tiribuzi, R., Crispoltori, L., Porcellati, S., Di Lullo, M., Florenzano, F., Pirro, M., Bagaglia, F., Kawarai, T., Zampolini, M., Orlacchio, A., Orlacchio, A., 2014. miR128 up-regulation correlates with impaired amyloid β (1–42) degradation in monocytes from patients with sporadic Alzheimer's disease. *Neurobiol. Aging* 35, 345–356. <https://doi.org/10.1016/j.neurobiolaging.2013.08.003>.
- Tomas Pereira, I., Burwell, R.D., Burwell, R.D., 2015. Using the spatial learning index to evaluate performance on the water maze. *Behav. Neurosci.* 129, 533–539. <https://doi.org/10.1037/bne0000078>.
- Uddin, M.S., Mamun, A.A., Labu, Z.K., Hidalgo Lanussa, O., Barreto, G.E., Ashraf, G.M., 2019. Autophagic dysfunction in Alzheimer's disease: cellular and molecular mechanistic approaches to halt Alzheimer's pathogenesis. *J. Cell. Physiol.* 234, 8094–8112. <https://doi.org/10.1002/jcp.27588>.
- Wang, X., Miao, Y., Abulizi, J., Li, F., Mo, Y., Xue, W., Li, Z., 2016. Improvement of electroacupuncture on APP/PS1 transgenic mice in spatial learning and memory probably due to expression of abeta and LRP1 in hippocampus. *Evid.-Based Compl. Alt.* 2016, 7603975. <https://doi.org/10.1155/2016/7603975>. [Chinese].
- Wang, H., Wang, R., Xu, S., Lakshmana, M.K., 2016. Transcription factor EB is selectively reduced in the nuclear fractions of Alzheimer's and amyotrophic lateral sclerosis brains. *Neurosci. J.* 2016, 1–8. <https://doi.org/10.1155/2016/4732873>.
- Wang, S.J., Wang, Q., Ma, J., Yu, P.H., Wang, Z.M., Wang, B., 2018. Effect of moxibustion on mTOR-mediated autophagy in rotenone-induced Parkinson's disease model rats. *Neural Regen. Res.* 13, 112–118. <https://doi.org/10.4103/1673-5374.224380>.
- Wu, L., Dong, Y., Zhu, C., Chen, Y., 2023. Effect and mechanism of acupuncture on Alzheimer's disease: a review. *Front. Aging Neurosci.* 15, 1035376. <https://doi.org/10.3389/fnagi.2023.1035376>.
- Xiao, Q., Yan, P., Ma, X., Liu, H., Perez, R., Zhu, A., Gonzales, E., Burchett, J.M., Schuler, D.R., Cirrito, J.R., Diwan, A., Lee, J.M., 2014. Enhancing astrocytic lysosome biogenesis facilitates Abeta clearance and attenuates amyloid plaque pathogenesis. *J. Neurosci.* 34, 9607–9620. <https://doi.org/10.1523/JNEUROSCI.3788-13.2014>.
- Xiao, Q., Yan, P., Ma, X., Liu, H., Perez, R., Zhu, A., Gonzales, E., Tripoli, D.L., Czerniewski, L., Ballabio, A., Cirrito, J.R., Diwan, A., Lee, J.M., 2015. Neuronally-targeted TFEB accelerates lysosomal degradation of APP, reducing A generation and amyloid plaque pathogenesis. *J. Neurosci.* 35, 12137–12151. <https://doi.org/10.1523/JNEUROSCI.0705-15.2015>.
- Xue, W.G., Ge, G.L., Zhang, Z., Xu, H., Bai, L.M., 2009. Effect of electroacupuncture on the behavior and hippocampal ultrastructure in APP 695 V 717 I Transgenic Mice. *Acupuncture Res.-zhen Ci Yan Jiu* 34, 309–314. CNKI: SUN: XCYJ.0.2009-05-004. [Chinese].
- Xue, W.G., Zhang, Z., Xu, H., Wu, H.X., Bai, L.M., 2011. Effect of electroacupuncture on learning-memory ability, and $\text{A}\beta$ and LRP 1 immunoactivity in hippocampal suicus microvessei in APP transgenic mice. *Zhen Ci Yan Jiu* 36, 95–100. <https://doi.org/DOI:CNKI:SUN:XCYJ.0.2011-02-005>.
- Yang, H., Li, J., Li, X., Ma, L., Hou, M., Zhou, H., Zhou, R., 2022. Based on molecular structures: amyloid- β generation, clearance, toxicity and therapeutic strategies. *Front. Mol. Neurosci.* 15, 927530. <https://doi.org/10.3389/fnmol.2022.927530>.
- Ye, Y., Zhu, W., Wang, X., Yang, J., Xiao, L., Liu, Y., Zhang, X., Liu, C., 2017. Mechanisms of acupuncture on vascular dementia—a review of animal studies. *Neurochem. Int.* 107, 204–210. <https://doi.org/10.1016/j.neuint.2016.12.001>.
- Yu, W.H., Kumar, A., Peterhoff, C., Shapiro Kulnane, L., Uchiyama, Y., Lamb, B.T., Cuervo, A.M., Nixon, R.A., 2004. Autophagic vacuoles are enriched in amyloid precursor protein-secretase activities: implications for β -amyloid peptide over-production and localization in Alzheimer's disease. *Int. J. Biochem. Cell Biol.* 36, 2531–2540. <https://doi.org/10.1016/j.biocel.2004.05.010>.
- Yu, W.H., Cuervo, A.M., Kumar, A., Peterhoff, C.M., Schmidt, S.D., Lee, J., Mohan, P.S., Mercken, M., Farmery, M.R., Tjernberg, L.O., Jiang, Y., Duff, K., Uchiyama, Y., Näslund, J., Mathews, P.M., Cataldo, A.M., Nixon, R.A., 2005. Macroautophagy: a novel β -amyloid peptide-generating pathway activated in Alzheimer's disease. *J. Cell Biol.* 171, 87–98. <https://doi.org/10.1083/jcb.200505082>.

- Yun, Y., Jang, D., Yoon, S., Kim, D., Choi, D., Kwon, O., Lee, Y., Youn, D., Park, W., 2017. Laser acupuncture exerts neuroprotective effects via regulation of Creb, Bdnf, Bcl-2, and Bax gene expressions in the hippocampus. *Evid.-Based Compl. Alt.* 2017, 7181637–17181611. <https://doi.org/10.1155/2017/7181637>.
- Zhang, Y., Tan, Y.X., Gao, Y.S., Yang, X.K., Li, C.L., Xue, W.G., 2022. Effects of electro-needling DU20 and KI1 on behavior and levels of dynein and CTSD in hippocampus of 6-month-old APP/PS1 double transgenic mice. *J. Clin. Acupuncture Moxibustion* 38, 67–73. <https://doi.org/10.19917/j.cnki.1005-0779.022078> [Chinese].
- Zhang, M., Xv, G.H., Wang, W.X., Meng, D.J., Ji, Y., 2017. Electroacupuncture improves cognitive deficits and activates PPAR-gamma in a rat model of Alzheimer's disease. *Acupunct. Med.* 35, 44–51. <https://doi.org/10.1136/acupmed-2015-010972>. [Chinese].
- Zhao, J., Ding, J., Huang, R., Wu, F., Li, H., 2019. Effect of electroacupuncture on expressions of Gas7 and NGF in arcular nucleus of rats with focal cerebral ischemia. *Zhōngguó Zhēnjiǔ* 39, 1205–1210. <https://doi.org/10.13703/j.0255-2930.2019.11.018>.
- Zheng, X., Lin, W., Jiang, Y., Lu, K., Wei, W., Huo, Q., Cui, S., Yang, X., Li, M., Xu, N., Tang, C., Song, J., 2021. Electroacupuncture ameliorates beta-amyloid pathology and cognitive impairment in Alzheimer disease via a novel mechanism involving activation of TFEB (transcription factor EB). *Autophagy* 17, 3833–3847. <https://doi.org/10.1080/15548627.2021.1886720>.
- Zheng, W., Su, Z., Liu, X., Zhang, H., Han, Y., Song, H., Lu, J., Li, K., Wang, Z., Chen, K., 2018. Modulation of functional activity and connectivity by acupuncture in patients with Alzheimer disease as measured by resting-state fMRI. *PLoS One* 13, e0196933–e. <https://doi.org/10.1371/journal.pone.0196933>.